JMEPEG (2004) 13:78-87
DOI: 10.1361/10599490417542

1059-9495/$19.00

Corrosion of Stainless Steels and Carbon Steel by Molten Mixtures of Commercial Nitrate Salts

S.H. Goods and R.W. Bradshaw

(Submitted 10 September 2003; in revised form 9 October 2003)

The isothermal corrosion behavior of two stainless steels and a carbon (C) steel in mixtures of $NaNO_3$ and KNO_3 was evaluated to determine if the impurities found in commodity grades of alkali nitrates aggravate corrosivity as applicable to an advanced solar thermal energy system. Corrosion tests were conducted for approximately 7000 hours with Types 304 and 316 stainless steels at 570 °C and A36 C steel at 316 °C in seven mixtures of $NaNO_3$ and KNO_3 containing variations in impurity concentrations. Corrosion tests were also conducted in a ternary mixture of $NaNO_3$, KNO_3, and $Ca(NO_3)_2$. Corrosion rates were determined by descaled weight losses while oxidation products were examined by scanning electron microscopy (SEM), electron microprobe analysis (EPMA), and x-ray diffraction (XRD). The nitrate mixtures were periodically analyzed for changes in impurity concentrations and for soluble corrosion products. Results of these tests indicated that the short-term corrosion rates of the stainless steel specimens in many of the mixtures could be described in terms of parabolic kinetics. However, no single rate law could be assigned to the corrosion kinetics resulting from exposure in all of the mixtures. For engineering applications, corrosion rates over the entire exposure period are best described as linear with respect to time. In the binary nitrate mixtures, the annualized rates of metal loss were found to be between 6 and 15 μm/year for the stainless steel specimens at 570 °C depending on the particular mixture. Metal loss for the C steel specimens immersed in these same mixtures at 316 °C extrapolated to approximately 1-4 μm/year. SEM and XRD revealed that the complex, multiphase surface oxides formed on the stainless steel coupons were composed primarily of iron-chromium spinel, iron oxides, and sodium ferrite. Magnetite was the principal corrosion product formed on the carbon steel specimens. Overall, for the typical range of impurities in commercially available nitrate salts, corrosion rates for solar thermal energy applications remained acceptable for all of the materials examined.

Keywords Containment, corrosion, nitrate salt, solar central receiver, stainless steel

1. Introduction

This work examines the isothermal corrosion behavior of primary containment materials that can be used in a solar central receiver power plant. Solar Two, a 10 megawatt (peak electric) demonstration facility, is a recent example of such an application and was undertaken as a joint project between a consortium of electric power utilities and the U.S. Department of Energy.[1] In a typical system, the receiver structure consists of a number of tubing panels through which circulates a heat transfer fluid that is heated by sunlight focused by an array of computer-controlled mirrors (heliostats). Based on earlier work, the heat transfer fluid is likely to be a molten nitrate salt consisting of 60 wt.% $NaNO_3$ and 40 wt.% KNO_3, which has a melting point of 238 °C and an intended working range of 290 to 570 °C.[2] These proportions of the individual nitrates were chosen because the resulting mixture optimizes a number of important properties, including heat capacity, thermal conductivity, corrosivity, ease of handling and storage, and cost.

It is expected that carbon (C) steel will be used to construct the low temperature portions of the system and a higher performance material, such as a stainless steel, will be used in high temperature portions (e.g., the receiver). We have chosen to examine A36 as the C steel and 304SS and 316SS as they represent likely and low cost candidates for each of these temperature regimes. The 300 series stainless steels are good choices for this study as previous work has shown that they exhibit good corrosion resistance and no degradation in mechanical properties after relatively long-term exposure to high-purity molten nitrates at the temperatures of interest.[3-5]

Large quantities of molten salt are needed to optimize the thermal energy storage capacity of this system. For example, the total inventory of salt in the Solar Two facility was about 1.5 million kilograms to provide thermal energy storage equivalent to several hours of peak electric power generation. Due to the very large salt inventory, it is important to select the most economical grades of these nitrates salts that satisfy the engineering requirements. A cost savings of nearly $1M dollars can be realized by choosing low-cost nitrates. Since these lower cost grades of nitrate can have higher impurity concentrations, it is necessary to assess their impact on containment material compatibility. The impurities typically present in some grades of nitrates, such as NaCl, $KClO_4$, Na_2SO_4, alkalinity, etc., must not aggravate corrosion of the containment alloys. For example, dissolved chloride may be a concern since it is often found to accelerate corrosion in high temperature oxidizing environments.[6]

While the previous studies referenced above have established that high purity nitrates constitute a relatively benign

S.H. Goods and **R.W. Bradshaw,** Materials and Engineering Sciences Center, Sandia National Laboratories, Livermore, CA, 94550. Contact e-mail: shgoods@sandia.gov.

Table 1 Nominal Composition and Source of the Constituents of Each Mixture Examined in This Study

Mixture	Composition	Source (Grade)
1 (low-chloride)	60% $NaNO_3$ 40% KNO_3	Coastal (a)
2 (high-chloride)	60% $NaNO_3$ 40% KNO_3 + 1.0 wt.% NaCl	Coastal
3 (max. chloride)	60% $NaNO_3$ 40% KNO_3 + 1.3 wt.% NaCl	Coastal
4	60% $NaNO_3$ 40% KNO_3	Chilean (b) (Technical) Chilean
5	60% $NaNO_3$ 40% KNO_3	Chilean (Industrial) Chilean
6	60% $NaNO_3$ 40% KNO_3	Chilean (Niterox) Cedar (c)
7	60% $NaNO_3$ 40% KNO_3	Chilean (Technical) Cedar
T (d)	$NaNO_3$ KNO_3 Ca $(NO_3)_2$	Coastal

(a) Coastal Chemical Co., Inc., Houston, TX
(b) Chilean Nitrate Corporation; Norfolk, VA
(c) Cedar Chemical Co., Vicksburg, MS
(d) Coastal HiTec XL, a proprietary mixture of Coastal Chemical Co.

corrosion environment, there is little specific information regarding the effects of impurities on corrosion resistance. The potential effects of salt impurities are illustrated in the work of Singh and Sen in which the effect of sulfate ion on corrosion of mild steel in nitrate melts was reported.[7] In this study, it was found that corrosion rates increased 20% when 7.5 wt.% Na_2SO_4 was added to nitrate salt melts. For chloride impurities, a few papers in the technical literature describe the results of short-term nitrate exposures, although at temperatures much higher than our application. The results generally indicate that chloride ion concentrations above 0.3 wt.% measurably increase corrosion rates of iron (Fe) and C steels compared with chloride-free melts.[8-10] Due to these findings, one specific goal of the current work was to address the question of increasing chloride concentration on corrosivity.

2. Experimental

2.1 Nitrate Mixtures

Seven binary mixtures and one ternary nitrate mixture were examined in this study and are listed in Table 1. All of the binary mixtures had the same nominal composition of 60% (wt.) $NaNO_3$ and 40% KNO_3. The first three mixtures were derived from a single source of relatively high purity salt. Mixtures #2 and #3 were composed of the same 60/40 mixture as #1 but with deliberate additions of chloride ion (as NaCl). The maximum chloride addition was 1.3 wt.%, which is 30% more than the highest expected level in commercial grades of salt. The intent of using these three mixtures was to systematically examine the effect of increasing chloride concentration on the corrosion behavior in the absence of significant amounts of other impurities.

Table 2 Impurity Concentrations (wt.%) in Nitrate Salt Mixtures (a)

Impurity	1	2	3	4	5	6	7
Chloride	0.040	0.574	0.760	0.260	0.462	0.104	0.060
Perchlorate	0.035	0.032	0.045	0.247	0.316	0.140	0.064
Sulfate	<0.002	<0.002	<0.002	0.146	0.182	0.015	0.011
Carbonate	0.010	0.01	0.006	0.009	0.021	0.009	0.010
Nitrite	0.025	0.028	0.027	<0.001	0.007	0.001	<0.001

(a) Nominal salt composition: 60 wt.% $NaNO_3$/40 wt.% KNO_3

Mixtures #4-7 were melted from other commercially available nitrates containing somewhat higher impurity concentrations. The sources and nominal composition of these mixtures are also shown in Table 1. In addition to these binary salt compositions, we have also examined the corrosivity of a ternary mixture chosen because it has an appreciably lower melting point (160 °C). The initial concentrations of some of the principal impurities in the nitrate mixtures used for the experiments are shown in Table 2. These values were determined using standard chemical analysis techniques. Since dissolved chloride may not be the only specie influencing the corrosion characteristics of the alloys studied, other potentially important impurities present in the nitrate mixtures, including perchlorate, sulfate, and carbonate, are listed. Finally, the initial concentration of nitrite (NO_2^-), an equilibrium constituent of the nitrate system, is also shown in Table 2.

2.2 Coupons

The nominal compositions of the test alloys, A36 carbon steel, 304SS, and 316SS, are shown in Table 3. Rectangular coupons measuring approximately 20 × 50 × 2 mm in thickness were cut from sheet stock, cleaned, alcohol rinsed, and weighed prior to immersion in the melts.

The A36 coupons were fully immersed in crucibles constructed from C steel. All of the stainless steel coupons were immersed in crucibles constructed of 304SS. Each crucible contained about 10 kg of the nitrate mixtures. The carbon steel specimens were immersed at 316 °C while the stainless steel specimens were immersed at 570 °C with the exception of the ternary mixture. The ternary mixture was intentionally maintained at a low temperature due to uncertainty regarding its thermal stability. This crucible was held below 480 °C for the first 5400 h and then gradually increased to 550 °C for the last 1600 h. In all cases, crucible temperature was controlled to ±10 °C. The melts were periodically sparged with air to maintain the nitrite concentration at the levels expected in solar thermal electric systems.

Two specimens of each alloy were removed from the nitrate mixtures at intervals of 120, 264, 480, 832, 1608, 2952, 4008, and 7008 h for examination and analysis. Descaled weight loss was used as the principal measure of corrosion to avoid ambiguities caused by surface oxides that may not be completely adherent. The C steel coupons were descaled by immersing them in an inhibited hydrochloric acid solution at room temperature,[11] while the stainless steel coupons were descaled in boiling alkaline permanganate.[12] These solutions removed all

Table 3 Nominal Elemental Composition of Alloys (wt. %)

Alloy	C	Mn	Si	Cu	Mo	Cr	Ni
A 36	0.29	0.85-1.20	0.15-0.30	0.20	…	…	…
304 SS	0.08	2.0	1.0	…	…	18-20	8-10
316 SS	0.08	2.0	1.0	…	2.0-3.0	16-18	10-14

corrosion products with negligible attack of the underlying metal. In some instances, the companion specimens for selected time intervals were cross-sectioned and prepared for metallographic examination. Optical and scanning electron microscopy (SEM) and electron microprobe analysis were used to characterize the structure and composition of the adherent corrosion products. The oxide phases present were identified by an x-ray diffraction procedure as described elsewhere.[13]

3. Results and Discussion

3.1 Stainless Steels

3.1.1 Descaled weight loss

316SS. Figure 1(a) shows a plot of the average (of two) descaled weight loss data versus time for 316SS. Weight loss measurements on duplicate coupons extracted from the salt mixtures at each time interval indicate that the scatter in the measurements was approximately 10% or less. The weight losses were between 5 and 6 mg/cm^2 after 7008 h of immersion, except for mixture #6, which was somewhat higher at 8 mg/cm^2. The weight losses at 7008 h correspond to reductions in metal thickness of 6-10 μm.

The close grouping of the weight loss curves for each of the salt mixtures indicates that corrosion of 316SS was relatively insensitive to the impurity content of the various nitrate mixtures. The small, descaled weight losses of coupons in the ternary salt mixture (#T) were due to the low temperature of that crucible until near the end of the test. The average values of the descaled weight losses of 316SS are plotted in Fig. 1(b) using logarithmic coordinates. When plotted in this way, weight loss versus time data can often be used to infer a corrosion mechanism. For example, data that exhibits one-half power time dependence implies that the surface corrosion products grow by a diffusion-controlled process where the rate of formation slows as the oxide film thickens. Such a "parabolic" process is inherently protective since the formation of the scale impedes further corrosion. Alternatively, linear kinetics can arise in a number of ways. In this instance, the corrosion film may be porous and therefore not constitute an effective diffusion barrier. Net linear kinetics may arise through a sequential process of protective oxide layer growth and spallation.

In the present experiments, we are unable to assign a power-law (i.e., a unique kinetic process) to most of the data. In many of the mixtures, kinetics appears to closely follow parabolic rate laws initially and then become linear after prolonged exposures. This situation often arises when oxide layers grow until their adhesion is compromised, by the formation of residual stresses in the oxide layer for example.[14] In the absence of uniform corrosion kinetics for the entire duration of these tests, a conservative approach based on a linear extrapolation of the data seems warranted for estimating corrosion-induced metal loss at longer times. For isothermal exposures, such linear extrapolations yield annualized weight losses of 6-10 mg/cm^2. It should be recognized that in a solar thermal power application, the receiver is only at temperature approximately 1/3 of the time. Thus, for a projected 30-year service life typical of solar thermal applications, an upper estimate of weight loss for 316SS is about 100 mg/cm^2. This corresponds to a total metal loss for 316SS of approximately 125 μm (0.005 in). We emphasize that these estimates are based solely on the current isothermal exposure data and do not account for effects that may arise from the diurnal cycling inherent in receiver operation.

304SS. Descaled weight loss measurements for the 304SS coupons versus time are plotted in Fig. 2(a). Overall, 304SS exhibited more variability in corrosion resistance compared with 316SS. The weight losses range from 4-10 mg/cm^2 after 7000 h of immersion or annualized losses of 5-12 mg/cm^2. These weight losses correspond to an annualized reduction in metal thickness of 6-15 μm. For a 30-year service life, an upper estimate of total metal loss for 304SS is approximately 150 μm (0.006 in). Again, the ternary mixture (#T) was an exception due to the singularly low temperature in that crucible until late in the test.

The weight loss data for 304SS reveal the presence of an effect due to chloride concentration. The effect is particularly evident for the high-purity mixture (#1) versus the chloride-doped mixtures, #2 and #3 (solid symbols in Fig. 2). The mixtures containing a variety of impurities, #4-7, also generally show increasing corrosion rates as chloride content increased, although other impurities, such as sulfate in mixture #5, may also affect corrosion rates.[15] Those mixtures containing less than approximately 0.3 wt.% chloride, #1, #6 and #7, experienced ~50% of the corrosion observed in the mixtures exceeding this level of chloride. We also note that corrosion rates of both 304SS and 316SS in the mixtures containing the lowest concentrations of impurities, #1, #6 and #7, were essentially identical.

All of the 304SS coupons exhibited relatively large weight losses of 1-2 mg/cm^2 within the first 100 h of exposure, followed by much slower rates of weight loss. These initial weight losses may be attributed to surface finish effects and may not be typical of the bulk material response. To determine the corrosion kinetics for the data shown in Fig. 2(a), it is necessary to normalize the data to remove the short-term weight losses. The normalization is performed by subtracting the time and weight loss measurements of the first exposure interval from all subsequent measurements. The relatively small weight losses, combined with the scatter in the data, preclude an unambiguous interpretation of Fig. 2(b), a logarithmic plot of the normalized data.

The normalized data do, however, reveal certain interesting trends that further suggest the presence of a chloride effect. The coupons exposed to the higher chloride concentration mixtures (#2-5) tend to exhibit nearly linear weight loss kinetics, although the rates are generally low. For the remaining low-chloride binary mixtures (#1, #6, and #7), the kinetics appears to more closely follow parabolic or one-half power time dependence. This can be seen more clearly in Fig. 3, which shows

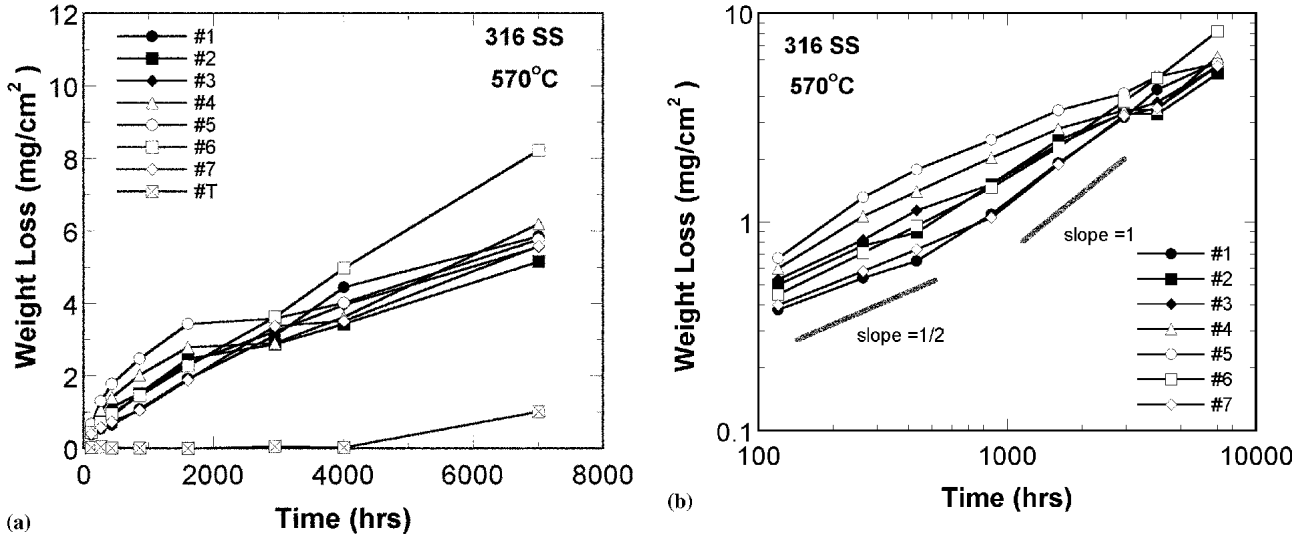

Fig. 1 **(a)** Descaled weight loss measurements for 316 stainless steel specimens exposed to nitrate salt mixtures at 570 °C; **(b)** logarithmic plot of descaled weight loss measurements shown in (a)

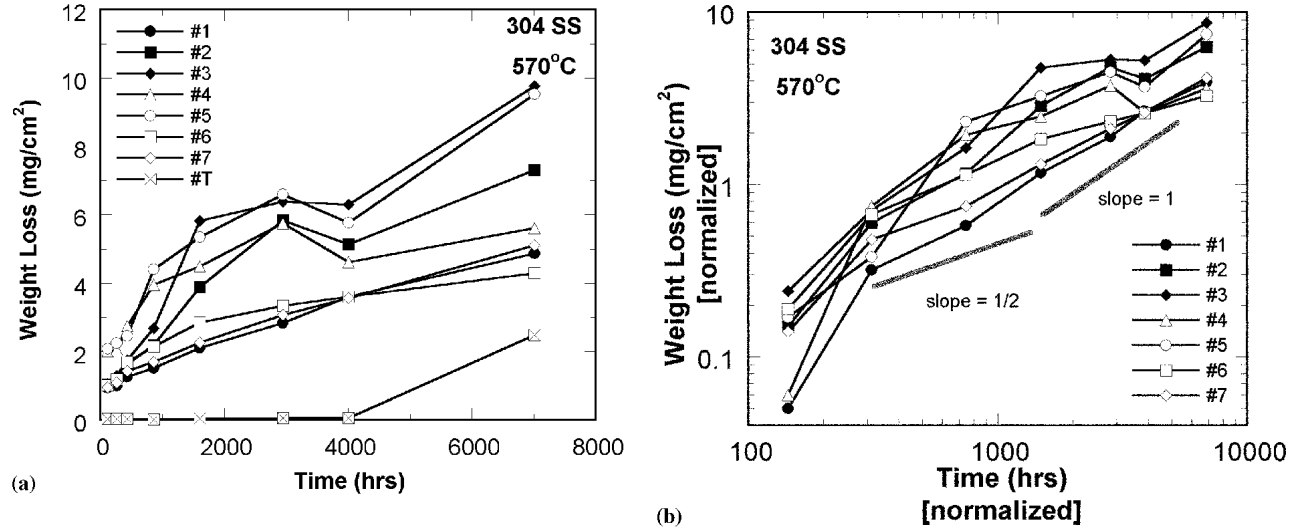

Fig. 2 **(a)** Descaled weight loss measurements for 304 stainless steel specimens exposed to nitrate salt mixtures at 570 °C; **(b)** logarithmic plot of descaled weight loss measurements shown in (a). To eliminate surface effects, the data have been normalized to exclude weight loss measurements from the first sampling interval.

a nearly linear relationship between descaled weight loss plotted against the square root of time (parabolic coordinates). This suggests that the corrosion scales formed in these low-chloride mixtures are protective. We suspect that the low linear corrosion rates in the higher chloride concentration mixtures are due to repeated detachment of otherwise protective oxides.

3.1.2 Oxide Scale Adherence. Visual inspection of the coupons before descaling clearly indicated that the surface oxide layers spalled to some degree on numerous samples. In many cases the unoxidized base metal was visible, indicating that spallation had occurred as the samples cooled to room temperature. Because both net weight change data and descaled metal loss data were obtained at corresponding time intervals, the tendencies of oxide scales to spall can be quantitatively evaluated. We define S to be the ratio of the net weight gain (the weight of a coupon upon removal from the crucibles minus its initial weight) and the descaled weight loss. If all of the oxide formed by corrosion adheres to a coupon and if the loss of metal alloy constituents as solutes in the melt is negligible, then the value of S is established by the stoichiometry of the oxide according to Eq 1.

$$S = \frac{g_O \times W_{(a/o)Oxygen}}{g_M \times W_{(a/o)Metal}} \quad \text{(Eq 1)}$$

In Eq 1, g_O and g_M are the stoichiometric coefficients of oxygen and metal of the oxide compound comprising the scale

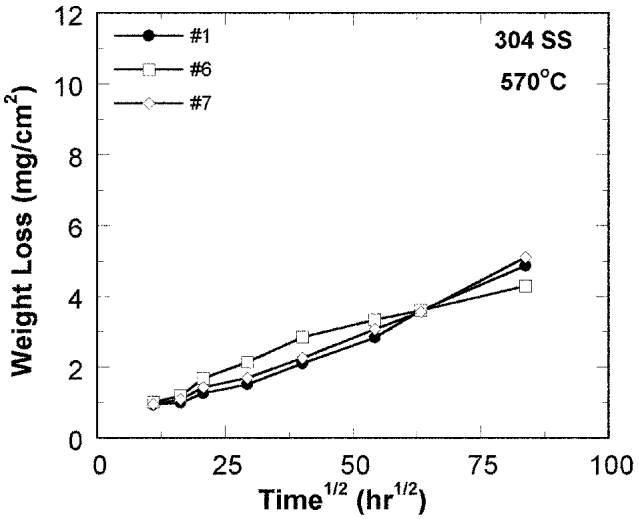

Fig. 3 Descaled weight loss for 304 stainless steel specimens exposed to nitrate salt mixtures 1, 6, and 7. After an initial rapid increase, weight loss measurements exhibit a parabolic dependence with respect to exposure time.

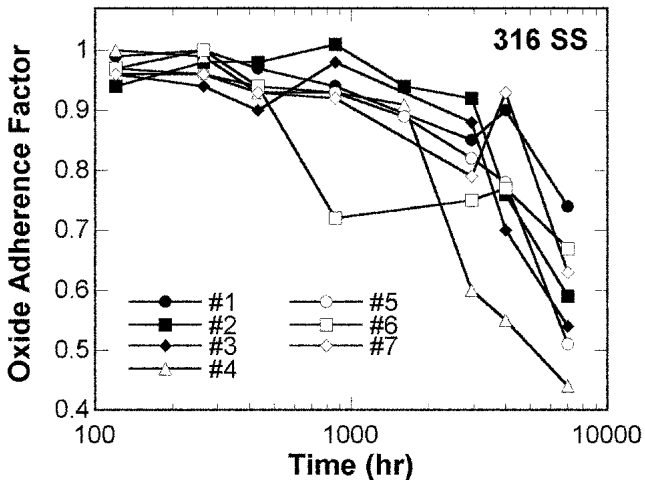

Fig. 4 Scale adherence factor for 316 SS. Data indicate that the surface oxides were adherent through 1600 hours of exposure.

and $W_{(a/o)Oxygen\ and}$ $W_{(a/o)Metal}$ are their respective atomic weights. Based on the x-ray diffraction (XRD) results discussed later, we assume that magnetite, Fe_3O_4, constitutes the major fraction of the oxide formed. For this case, the value of S is 0.38. Spinel [$Fe(Fe,Cr)_2O_4$] was also formed, but the value of S changes marginally as the transition metals Fe and chromium (Cr) have comparable atomic weights.

To obtain an indicator of oxide adherence that varies between unity for completely adherent layers and zero for completely detached oxides, we note that for completely adherent oxides, the weight of a coupon as removed from the melt, W_f, is

$$W_f = W_o + S\,(\Delta W_{loss})$$

where W_o is the initial coupon weight. To obtain a quantity on the left-hand side that becomes zero if all the oxide spalls off, we subtract the weight of the descaled coupon, W_d, from each side.

$$(W_f - W_d) = (W_o - W_d) + S\,(\Delta W_{loss}) = (S + 1)\,(\Delta W_{loss})$$

The above equation can be rearranged into an identity that we define as the scale adherence factor, Y.

$$Y = \frac{1}{S+1}\frac{(W_f - W_d)}{\Delta W_{loss}} \qquad \text{(Eq 2)}$$

We expect that oxide scales should be adherent at short times, so the sampling time at which Y decreases below unity indicates that oxide spallation has occurred. Because weight change measurements are aggregated over the entire coupon, the value of the indicator gives no information about the type of spallation and is not necessarily useful for mechanistic interpretations of spalling. Values less than unity does not serve to indicate that spallation occurs concurrently with the high temperature exposure or at some time subsequent to exposure. A similar approach has been used recently by Ziemniak and Hanson to determine the adherence of oxide layers formed on Alloy 625 during long-term exposure to high-temperature steam.[22] The "corrosion release factor" used by these authors is essentially the complement of the "scale adherence factor" defined here.

The calculated values of Y for 316SS and 304SS are shown in Fig. 4 and 5 versus log time. Figure 4 shows that the oxide layers on 316SS are adherent in all the salt mixtures for at least 1600 h, except for mixture #6. At the next sampling interval (2952 h), these values decline below unity in all cases. This result correlates with the weight loss measurements in Fig. 1(a) and 1(b) in that parabolic kinetics are obeyed at short time intervals while linear kinetics hold for longer-term exposures. In contrast to 316SS, Fig. 5 shows that even at 100 h, the oxide layers on 304SS were not completely adherent. The lack of oxide adherence indicated in Fig. 5 is not inconsistent with the parabolic weight change data for 304SS shown in Fig. 3 for mixtures #1, #6, and #7. Rather, these two observations suggest that the loss in oxide adherence results from thermal stresses induced upon specimen cooling to room temperature, rather than oxide growth stresses.

3.1.3 Oxide Structure and Composition. Detailed characterization of the structure and evolution of the corrosion products was made difficult due to the degree of spallation that occurred and by the complexity of the surface oxidation products. Notwithstanding these difficulties, remnant oxide scales from several coupons provided useful information regarding structure. Figure 6 shows a scanning electron micrograph (SEM) of a metallographic cross-section of a 304SS coupon immersed in mixture #4 for 1608 h. The coupon was nickel (Ni) plated prior to metallographic preparation (to protect the corrosion products from damage) and the layer of plating is marked on the micrograph. The microscopy reveals that the oxide has formed a surface film with an average thickness of 5-12 μm. The scale in Fig. 6 is composed of two distinct regions separated by a well-defined crack that runs parallel to

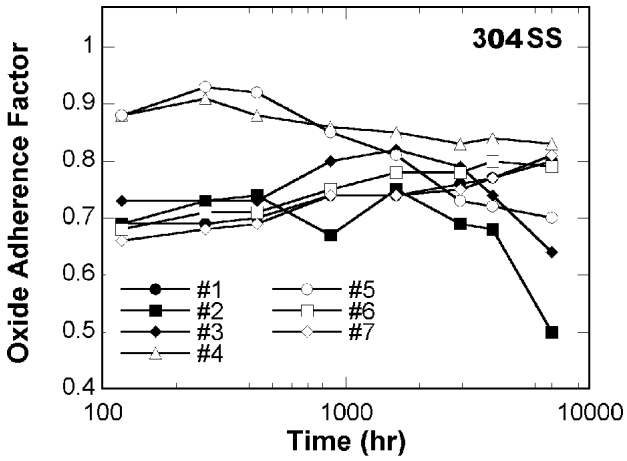

Fig. 5 Scale adherence factor for 304 SS. Data indicate that the surface oxides were not adherent even at short times.

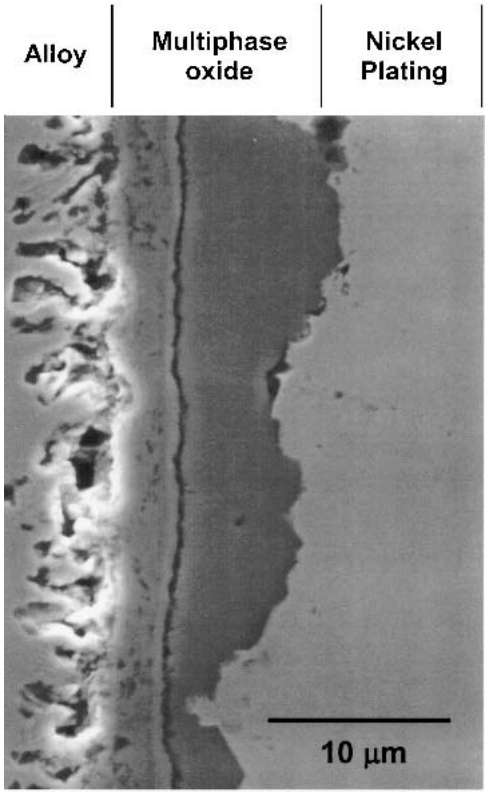

Fig. 6 Scanning electron micrograph of a metallographic cross-section of a 304SS coupon immersed in mixture #4 for 1608 h

the oxide-metal interface. The scale formed at the external surface (adjacent to the nickel layer) is the most irregular in thickness, varying from 1 to 8 μm. The variability in the thickness of the oxide reflects the lack of adherence (it is likely that the structure shown is not a first generation scale). While the oxide adjacent to the alloy is considerably more uniform in thickness, it appears to be quite porous. The general morphology of the corrosion products shown in this figure was characteristic of those formed in each of the binary salt mixtures. However, the extensive porosity at the oxide-metal interface evident in Fig. 6 was only occasionally observed. It was not seen in any of the 304SS coupons at times shorter than 1608 h and was observed in the 316SS specimens at only much longer times. This porosity may explain the lack of adherence of the corrosion products. The fact that this porosity is only occasionally observed suggests it develops slowly with time as each successive generation of oxide is formed.

Figure 7 shows a backscatter electron image (BSE) of the adherent oxide on a 304SS coupon immersed in mixture #1 for 7008 h. The contrast in the corrosion layer reflects the sensitivity of BSE to the atomic mass of the constituents of the different oxide phases. The figure also shows the elemental distribution of the principal alloying elements of 304SS and certain constituents of the nitrate mixture,[16] sodium and magnesium, through the thickness of the surface scale. This analysis was done using the wavelength dispersive analysis (WDS) capability of the electron microprobe (EMP) and is semi-quantitative in nature. Due to the extensive spallation, neither the image nor the elemental profiles reflect the structure and composition of a 7000 h oxide. Rather, they only reflect the residual, adherent structure of an n^{th} generation scale. Thus, these elemental profiles can show considerable variation between specimens. For the corrosion features shown in Fig. 7, the WDS results reveal that the oxide at the external surface (the surface in contact with the salt) was a Cr-free, Fe-based oxide that contained ~12% sodium. This is typical of many of the residual oxides at this and at shorter time intervals and has been observed in an earlier study.[17] X-ray diffraction (see below) identified this surface scale as $NaFeO_2$. The analysis further revealed that Fe and Cr were the principal metallic constituents of the subsurface scale. Manganese (Mn) was also found in this layer at 2-3 times its normal concentration in the alloy. Chemical analysis revealed that mixture #1 contained only trace amounts of magnesium (Mg) and in agreement with this, no magnesium Mg was detected in any of the oxide layers.

XRD was used to identify specific crystallographic phases in the oxide structures. The analyses focused primarily on samples removed from mixtures #1 and #5 at progressively longer sampling times up to 2952 h. Three major phases were identified on both alloys. These consisted of an orthorhombic Fe_2O_3 (hematite) type phase, a cubic spinel Fe_3O_4 (magnetite) type and orthorhombic sodium ferrite, $NaFeO_2$. The sodium ferrite may have its origin in the reaction between trace amounts of sodium oxide in the molten nitrate and hematite as

$$Na_2O + Fe_2O_3 \rightarrow 2NaFeO_2$$

Based on the corresponding EMP data, Cr and Mn likely substitute for iron in the cubic spinel oxide corresponding to an $(Fe, Cr, Mn)_3O_4$ type structure. In addition, it is likely that substitution of Mg (when present) and Cr for Fe in the spinel Fe_3O_4 phase corresponds to a $(Fe, Cr, Mg)O_4$ type cubic structure. Where Mg is detected, it is likely that Mg^{+2} substitutes for Fe^{+2} in Fe_3O_4 to form $MgFe_2O_4$.

Coupons immersed in mixtures #4 and #5 had surface scales

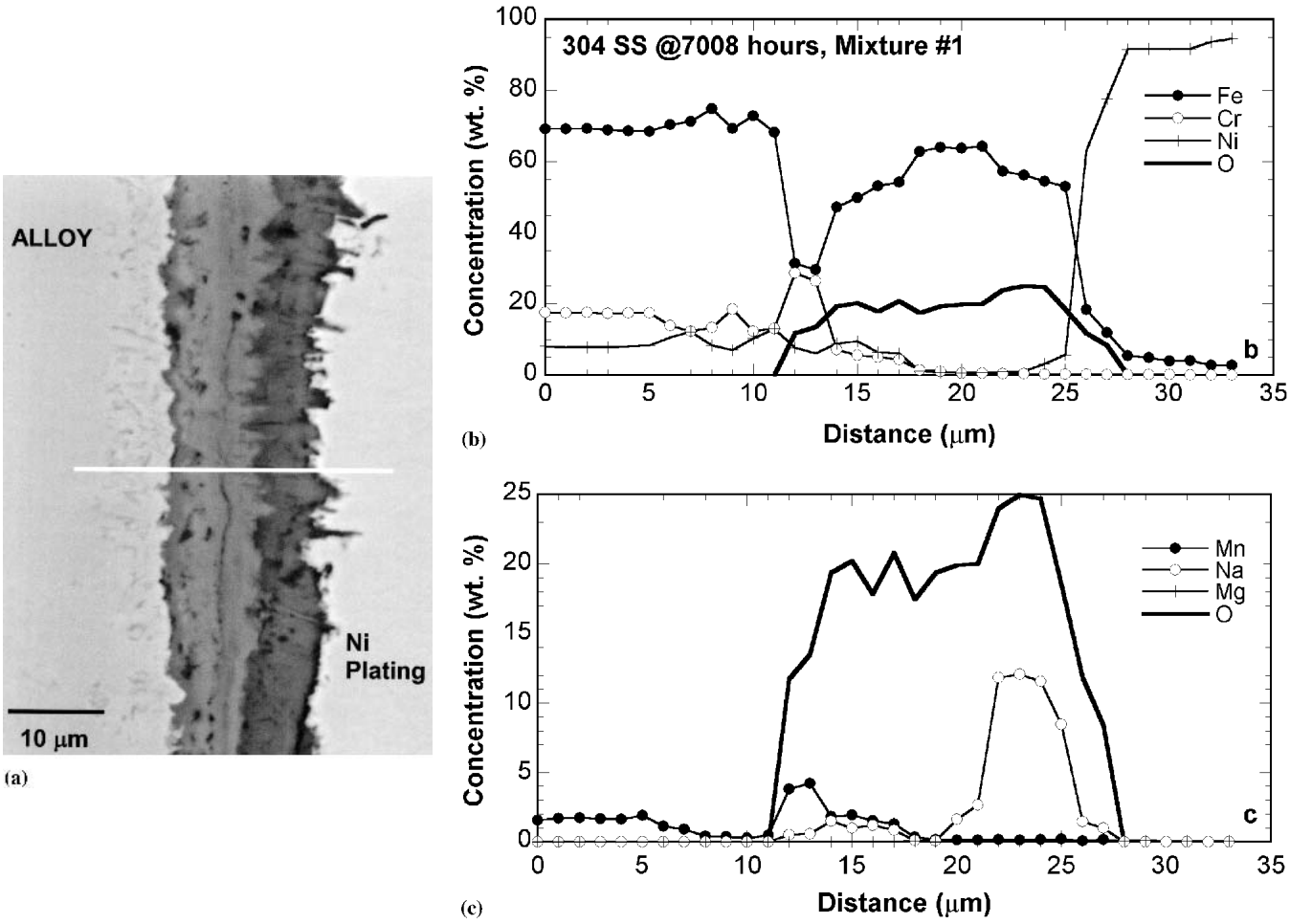

Fig. 7 Backscatter electron image (BSE) of the adherent oxide on a 304SS coupon immersed in mixture #1 for 7008 h

with a distinctive rust-red coloration indicative of hematite (Fe_2O_3). The relative abundance of the different phases changed with immersion time. For instance, the XRD results for the samples immersed for 864 h identified the presence of both the Fe_2O_3 and Fe_3O_4 type of oxides. At this sampling interval, Fe_2O_3 was more abundant compared with Fe_3O_4, based on relative intensity of the diffraction peaks. The Fe_3O_4 phase increased with respect to Fe_2O_3 as exposure time increased. $NaFeO_2$ was first observed for the 1608 h samples (both 304 and 316SS) and was most abundant in the samples removed from mixture #5. Furthermore, the $NaFeO_2$ phase continued to increase in samples removed at 2952 h. Due to the extensive spallation, x-ray analysis was not performed at longer immersion times. Even at shorter times, the observations regarding the relative abundance of the different oxide phases must be considered qualitative.

All of the 304SS coupons exhibited the presence of dark subsurface features located in a 5 μm wide band immediately below the oxide-metal interface. In each instance, these features are associated with elevated Ni concentrations (≈14-20 wt.%) and depleted Cr concentrations (~12%).

The oxide structures formed on a 316SS coupon exhibited similar features to those shown for the 304SS coupons.

3.2 Carbon Steel

3.2.1 Descaled weight loss. Descaled weight loss measurements for the carbon steel specimens at 316 °C are shown in Fig. 8(a). In general, the data fall into two distinct categories. The specimens exposed to the high-purity/chloride-doped mixtures (#1-3) experienced both larger initial weight losses and larger long-term weight losses than coupons immersed in mixtures #4-7, which contained a variety of impurities in addition to chloride. Chloride concentration alone cannot account for these differences in corrosivity since the chloride levels of mixtures #4-7 were intermediate between mixtures #1 and #2 (see Table 1). Indeed, even for those specimens immersed only in mixtures #1, #2, and #3, where the base nitrate composition was identical, the increasing chloride concentration did not result in an unambiguous increase in corrosion. For the specimens exposed to nitrate mixtures containing other impurities (#4-7), the overall weight changes do not show a systematic effect of chloride levels on corrosion.

These observations contrast with previous findings of short-term corrosion tests. For example, El Hosary, et al.,[8] reported that the corrosion rate of mild steel at 400 °C increased approximately as the logarithm of the chloride concentration in

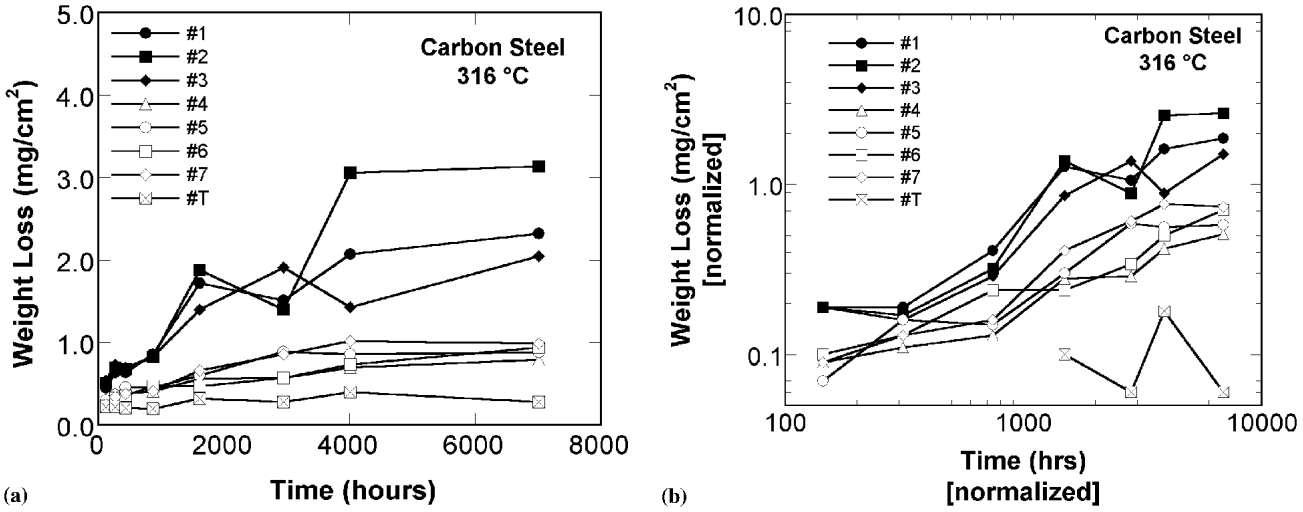

Fig. 8 **(a)** Descaled weight loss measurements for carbon steel specimens exposed to nitrate salt mixtures at 316 °C; **(b)** logarithmic plot of descaled weight loss measurements shown in (a). To eliminate surface effects, the data have been normalized to exclude weight loss measurements from the first sampling interval.

the range studied here. In that work, at 0.5 wt.% chloride, the corrosion rate increased by a factor of about three compared with a chloride-free melt during an 8 h test. Notoya, et al., report substantially the same results for corrosion of iron at 400-450 °C.[10] The lower temperatures used in the current work may be the source of the contrasting behavior.

Figure 8(b) is a logarithmic plot of the weight loss data shown in Fig. 8(a). Similar to the behavior of the 304SS, all of the carbon steel coupons exhibited a relatively large weight loss in the first sampling interval, ranging between 0.2 and 0.5 mg/cm^2. As before, it is necessary to normalize the data to remove the short-term effects to identify the corrosion kinetics. Here too, the small weight change measurements coupled with the scatter in the data preclude unambiguous interpretation of Fig. 8(b). However, the coupons exposed to mixtures #1-3 tend to exhibit nearly linear weight loss kinetics. For the remaining binary mixtures (#4-7), the kinetics appear to more closely follow parabolic or one-half power kinetics, suggesting an oxidation process that yields more protective scales than for the first three mixtures. Other studies have shown that carbon steels can display parabolic oxidation kinetics in molten nitrates during short (10 h) immersion times.[8-10]

3.2.2 Oxide Adherence on Carbon Steel. In contrast to the stainless steel coupons, the carbon steel coupons did not show any spallation of oxides to the bare metal upon visual examination. To estimate the amount of spallation, the same protocol used above was applied to the weight change data obtained for carbon steels. The results of these calculations are presented in Fig. 9 and generally show that oxides on the C steel specimens immersed in mixtures #4-#7 are adherent even after 7000 h of immersion. This adherence is no doubt partly due to the relatively thin layers that grow at the lower temperature of these tests. Thinner layers generate both lower growth stresses as well as lower thermally-induced stress upon cooling. The calculated adherence factors for the specimens immersed in mixtures #1-#3 are somewhat less than unity and the weight loss data presented in Fig. 8(b) indicate that the corrosion kinetics are more accurately described as linear.

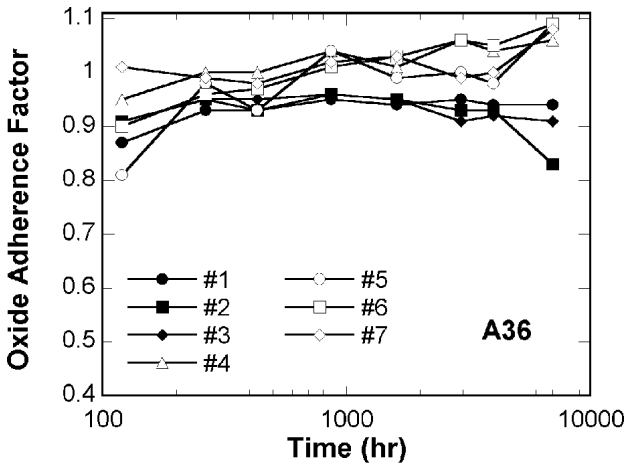

Fig. 9 Oxide adherence factor for carbon steel specimens. Data indicate that the surface oxides were generally adherent at this relatively low exposure temperature.

The rather low amounts of corrosion rendered microscopy ineffective as an analytical tool for characterizing the structure and composition of the residual corrosion products simply because the oxide scales were only 2-4 μm in thickness, based on weight change data. However, XRD showed the scale to consist of two phases, a dominant Fe_3O_4 spinel phase and a minor phase corresponding to Fe_2O_3.

We have not discussed the structure and composition of the oxide layers formed on the alloys immersed in the ternary mixture. This is due principally to the minimal corrosion experienced by all the stainless steels at the low exposure temperature. The very thin surface scales formed on the stainless coupons precluded any quantitative or even qualitative analysis of the type discussed above. We note however, that the A36 coupons exposed to the ternary mixture (#T) exhibited lower weight losses than those in any of the binary mixtures at the same temperature. It was evident that a different type of oxide

was formed on C steel in the ternary salt since it was difficult to descale these coupons compared with the others.

3.3 Molten Salt Composition

The concentrations of the impurity species listed in Table 2 and dissolved metallic corrosion products were analyzed periodically. A detailed discussion of molten salt chemistry and the changes in composition of the impurities in the molten salt mixtures during these experiments is available elsewhere.[21] With regard to the discussion of corrosion in this paper, we note that the molten salt mixtures maintained concentrations of nitrite ion consistent with equilibrium calculations for the nitrate-nitrite-oxygen shift reaction given contact with air at the temperatures used for corrosion testing.[18] This reaction increased the concentration of nitrite to about 3.6 wt.% at 570 °C. The amount of nitrite at 316 °C was negligible.

The chloride concentrations in a number of mixtures increased slightly during the first 1608 h of the test. The increases in chloride occurred in concert with a corresponding and stoichiometric decrease in perchlorate (ClO_4^-) concentration until, at 1608 h, the perchlorate concentration in all of the high temperature crucibles was essentially zero. The chloride levels then stabilized at the higher values. Although the perchlorate ion is reported to be stable in KNO_3 at 450 °C,[19] it can be reduced to chloride by a number of reactions. A redox reaction would likely occur with nitrite since a stoichiometric excess of nitrite is formed by the shift reaction mentioned above. The free energy change for perchlorate reduction by nitrite is favorable based on the data available for low temperature.[20] Perchlorate can also be reduced by metallic corrosion or by other impurities in the melts. The rate of perchlorate reduction was much slower at 316 °C.

Molten salt samples from each high temperature crucible were analyzed for dissolved Cr and Mg as the hexavalent oxidation products of these alloying elements (chromates and manganates) are soluble in molten nitrates.[2] Figure 10 shows the increase in Cr concentration with time. After initially increasing up to 864 h, the Cr concentration remained nearly constant, suggesting that the solubility limit of an unidentified metallic chromate compound was reached. The Mn concentration continued to increase with time although at a much lower level than Cr due to its relatively low concentration in the alloys. Analyses for Fe and Ni were not performed, as these elements do not form soluble species in molten nitrate salts.[2]

4. Summary

The experimental data presented here show that the impurities typically contained in commercial grades of alkali nitrates have relatively small effects on corrosion of stainless and carbon steels in molten salts prepared from these constituents. The corrosion rates of 316SS and 304SS imply that metal losses of 6-15 μm/year may be anticipated during isothermal service at 570 °C. For the 304SS coupons, the influence of increasing chloride concentration was evident; namely, the rate of weight loss increased as the chloride concentration increased. However, the magnitude of the effect was not significant in the context of the engineering application. No single rate law could

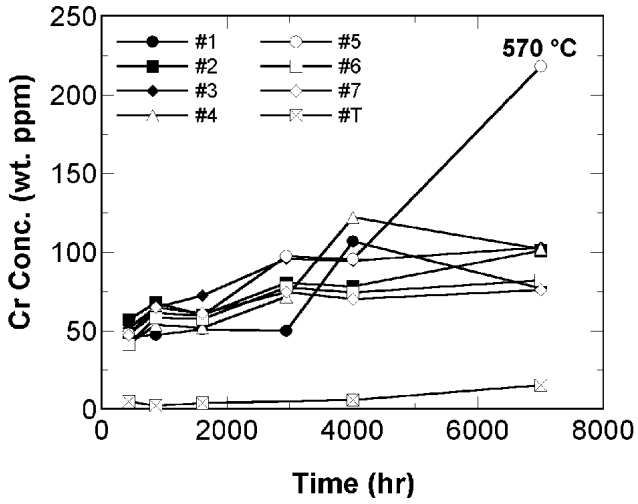

Fig. 10 Chemical analysis of concentration of dissolved chromium in the molten nitrate salt mixtures during the corrosion tests at 570 °C

be ascribed to the corrosion kinetics for the alloy in all of the mixtures. The low-chloride mixtures tended to exhibit parabolic kinetics while the remainder of the mixtures exhibited approximately linear kinetics. For 316SS, weight loss generally followed parabolic corrosion kinetics at short times, transitioning to linear kinetics at longer exposure times. Corrosion rates for 316SS were largely insensitive to the impurity content of the melts. Elemental analysis of the corrosion products on the stainless steel coupons revealed that they consisted of a complex mixture of iron-based oxides that contained several other elements derived from both the alloying elements (Cr, Mn) and constituents of the molten salt (Na, Mg).

The differences between the corrosion behavior of the two types of stainless steel tested may well arise from differences in the initial surface finish of the test coupons or from minor differences in their elemental compositions.

Neither the incomplete oxide adherence of the stainless steel samples nor the gradual evolution of porosity in the alloys immediately below the surface scale has been previously observed. These particular results indicate the need to conduct corrosion tests using non-isothermal conditions to obtain reliable estimates of corrosion allowances for components such as receiver tubes that necessarily undergo daily thermal cycling between the maximum and ambient temperatures. These tests are in progress at this time.

The experimental data demonstrate that at 316 °C, A36 carbon steel is relatively tolerant to the impurities typically found in commodity grades of alkali nitrates. The influence of deliberate additions of chloride to a high-purity nitrate mixture was not clearly evident. While there appears to be some difference in the corrosion behavior among various salt mixtures, the overall weight losses were modest and correspond to corrosion rates of about 5 μm/year. Oxide layers, which consisted primarily of magnetite, were generally adherent during these long-term tests.

Acknowledgments

The authors wish to acknowledge the contribution of the following individuals: A.D. Gardea, and D.R. Boehme (SNL/

CA), and, M.R. Prairie and J.M. Chavez (SNL/NM). This work was supported by the U.S. Department of Energy under contract DE-AC04-94AL85000.

References

1. P.J. Speidel, B.D. Kelly, M.R. Prairie, J.E. Pacheco, R.L. Gilbert and H.E. Reilly: "Performance of the Solar Two Central Receiver Power Plant," *J. Phys. IV*, 1999, *9,* pp. 181-87.
2. R.W. Bradshaw and R.W. Carling, *A Review of the Chemical and Physical Properties of Molten Alkali Nitrate Salts and Their Effect on Materials Used for Solar Central Receivers,* SAND87-8005, Sandia National Laboratories, Livermoe, CA, April 1987.
3. R.W. Bradshaw, *Corrosion of 304SS by Molten $NaNO_3$-KNO_3 in a Thermal Convection Loop,* SAND80-8856, Sandia National Laboratories, Livermore, CA, Dec. 1980.
4. S.H. Goods: *J. Mater. Energy Sys.,* 1983, *5,* pp. 28-36.
5. S.H. Goods: "Mechanical Properties of Alloy Steels in Molten Sodium-Potassium Nitrate Salts," *High Temperature Corrosion in Energy Systems,* M.F. Rothman, ed., The Metallurgical Society of AIME, Philedephia, PA, 1985, pp. 643-58.
6. P. Hancock: *Oxid. Metals*, 1985, *23,* pp. 305-11.
7. I.B. Singh and U. Sen: *Brit. Corros. J.*, 1992, *27,* pp. 299-304.
8. A.A. El Hosary, A. Baraka, and A.I. Abdel-Rohman: *Brit. Corros. J.*, 1976, *11,* pp.228-230.
9. A. Baraka, A. I. Abdel-Rohman, and A.A. El Hosary, *Brit. Corros. J.*, 1976, *11,* pp. 44-46.
10. T. Notoya, T. Ishikawa, and R. Midorikawa: "Corrosion Behavior of Iron and Low Carbon Steels in Molten Alkali Nitrates Containing Alakali Halide" in *Proc. Fifth Int'l. Congress on Metallic Corrosion*, N.A.C.E., Houston, TX, 1972, pp. 1039-143.
11. I. Kayafas: *Corrosion*, 1980, *36,* pp. 443-45.
12. N.A.C.E. Technical Practices Committee: "Procedures for Quantitative Removal of Oxide Scales Formed in High temperature Water and Steam," *Mater. Performance*, 1967, *6,* p. 69-72.
13. R.W. Bradshaw, S.H. Goods, M.R. Prairie, and D.R. Boehme: "Corrosion of Carbon Steel and Stainless Steels In Molten Nitrate Mixtures" in *Proceedings of the International Symposium on Molten Salt Chemistry and Technology—1993,* M.L. Saboungi and H. Kojima, ed., PV-93-9, The Electrochemical Society, Pennington, NJ, 1993, pp. 446-51.
14. J. Armitt, D. R. Holmes, M. I. Manning, D. B. Meadowcroft, and E. Metcalfe: "The Spalling of Steam Grown Oxide from Superheater and Reheater Tube Steels," Central Electricity Generating Board (UK), RD/L/R 1974 (Feb. 1978).
15. Martin-Marietta Corp., "Alternate Central Receiver Power System, Phase II," Final Report, Vol. III–Molten Salt Materials Tests, SAND81-8192/3, Jan. 1984, Sandia National Laboratories, Albuquerque, NM.
16. Chemical Composition Specifications, Chilean Nitrate Corporation, Norfolk, VA, 1984.
17. D.R. Boehme and R.W. Bradshaw: *High Temp. Sci.,* 1984, *18,* pp. 39-51.
18. D.A. Nissen and D.E. Meeker: *Inorg. Chem.,* 1983, *22,* pp. 716-21.
19. O.J. Kleppa and S.V. Meschel: *J. Phys. Chem.,* 1963, *67*, p. 2750-55.
20. I. Barin, O. Knacke, and O. Kubachewski: "Thermochemistry of Anion Mixtures in Simple Fused Salt Systems" in *Thermochemical Properties of Inorganic Substances*, Springer-Verlag, Berlin, Germany, 1977.
21. S.H. Goods, R.W. Bradshaw, M.R. Prairie, and J. M. Chavez, *Corrosion of Stainless and Carbon Steels in Molten Mixtures of Industrial Nitrates,* SAND94-8211, Sandia National Laboratories, Livermore, CA, March 1994.
22. S.E. Ziemniak and M. Hanson: *Corros. Sci.,* 2003, *45*, pp. 1595-1618.